Jour. Research U.S. Geol. Survey
Vol. 2, No. 6, Nov.-Dec. 1974, p. 743—751



# FLASHING FLOW IN HOT-WATER GEOTHERMAL WELLS

By MANUEL NATHENSON, Menlo Park, Calif.

*Abstract.*—The production characteristics of hot-water geothermal wells which flash to steam-water mixtures in the cased part of the hole were analyzed. The flashing flow is assumed to be isenthalpic and, for purposes of calculating pressure drop, a finely dispersed mixture of equal average velocity. Water flow in the aquifer is treated using steady, radial Darcy flow. Calculations for a typical geothermal well show the effects on production of varying the system parameters of aquifer permeability, depth to water table, and base temperature. Field data from Wairakei, New Zealand, demonstrate the reductions in flow caused by mineral deposits in the bore. Data from Imperial Valley, Calif., agree well with calculated results.

The flow characteristics of wells tapping hot-water geothermal systems are important to utilization of geothermal energy. The purpose of this work is to use an approximate formulation of the fluid mechanics of flashing steam-water mixtures to study the effects of various geothermal reservoir parameters on the production characteristics at the wellhead. The fluid mechanics and thermodynamics are formulated in the first section. Calculated results are presented and discussed in the second section. Some field data from Wairakei, New Zealand, and Imperial Valley, Calif., are analyzed in the third section.

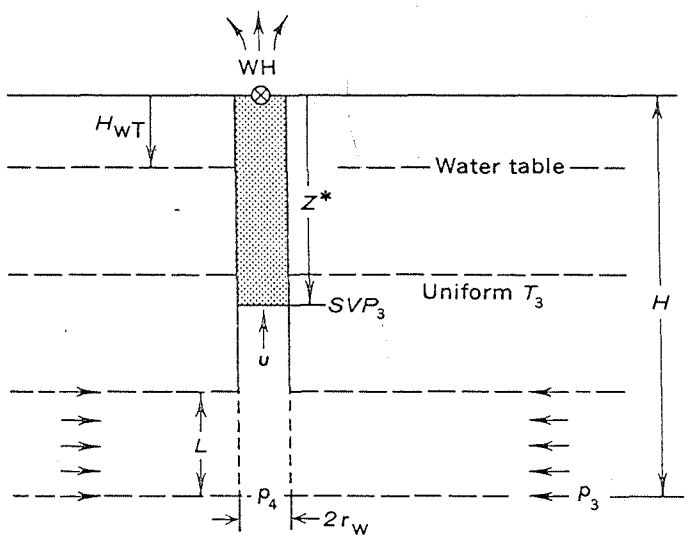


Figure 1.—Schematic diagram of flashing-flow system (exaggerated horizontally). $H$, well depth; $p_3$, aquifer pressure; $p_4$, well flowing pressure; $SVP_3$, saturated vapor pressure; $r_w$, well radius; $H_{WT}$, depth to water table; $Z^*$, level where boiling begins; WH, wellhead; $u$, flow speed of mixture; $L$, thickness of aquifer; $T_3$, temperature of water in aquifer.

## PROBLEM FORMULATION

The physical situation is diagrammatically represented in figure 1. An aquifer of thickness $L$ contains hot water at temperature $T_3$ with pressure $p_3$ at the datum level $H$ (which corresponds to the well depth). The well either erupts spontaneously when the valve at the wellhead is opened or is induced to erupt (White, 1968). The steady state involves flow of water in the aquifer and up the well until a level $Z^*$ is reached where the hydrostatic pressure has decreased sufficiently for boiling to commence (saturation pressure $SVP_3$, corresponding to the temperature $T_3$). The pressure continues to decrease up the well in the two-phase regime, but the rate of change decreases upward as the proportion of vapor increases; and the density decreases. The driving force for the flow is the lower weight of the steam-water mixture from the level $Z^*$ to the surface relative to that of the undisturbed aquifer calculated at a datum equal to $Z^*$. The quantity of flow and the wellhead pressure can be controlled within certain limits by a throttling valve or orifice plate at the surface. The problems of two-phase flashing flow and bore-hole characteristics were discussed in a general way by Bodvarsson (1951). The formulation that follows is based on the work of Elder (1965).

Assuming that the waterflow in the aquifer is perfectly radial Darcy flow, the total mass flow $M$ into the well is related to the pressure drop from the aquifer pressure $p_3$ (at the datum $H$) to the well pressure $p_4$ (at the same datum) by

$$M = \frac{2\pi LK}{V_{w3}\mu} \frac{(p_3 - p_4)}{ln(r_e/r_w)}, \qquad (1)$$

where $K$ is the permeability, $\mu$ and $V_{w3}$ are the viscosity and specific volume of water at the aquifer temperature, $r_e$ is the

radius of drainage, and $r_w$ is the well radius (Muskat, 1946). Equation 1 assumes that no flashing occurs in the aquifer. Because of the complications of adding several more parameters to the problem, flashing in the aquifer is not considered here. Note, however, that flashing flow in the porous medium significantly lowers the permeability as compared to that for all-liquid flow.

As water flows into and up the well, the hydrostatic pressure becomes low enough at the level $Z^*$ for boiling to begin. The saturated vapor pressure $SVP_3$ at the level $Z^*$ is related to the bottom-hole flowing pressure $p_4$ through hydrostatic equilibrium by

$$SVP_3 = p_4 - \frac{g}{V_{w3}}(H - Z^*), \tag{2}$$

where $g$ is the acceleration of gravity. Neglected factors include the hydrodynamic resistance when there is only liquid water in the bore, conductive transfer of heat from the well to the surrounding rocks, and the partial pressures of dissolved gases.

Above the level $Z^*$, the flow of the flashing mixture is complicated. A reasonable approximation for flashing flow can be made by treating it as a finely divided mixture with equal average velocities of liquid and vapor when calculating the hydrodynamic resistance, including the changing proportions in the mass conservation and energy equations (Allen, 1951). This approximation neglects any slip of liquid relative to the vapor and is better at higher flow rates where the fluid is well mixed owing to turbulence. James (1968) has looked at the annular dispersed regime of two-phase flashing flow in a pipe and suggested certain modifications to the following formulation. If sufficiently detailed physical data on flashing discharges were available, it would be worthwhile to verify his suggestion; the published data for bore holes is too meager to warrant the additional complication.

Using the volume fraction of water $X$, conservation of mass at any section is

$$\frac{u}{V} = \left(\frac{X}{V_w} + \frac{(1-X)}{V_g}\right) u = \frac{u^*}{V_{w3}} = \frac{M}{\pi r_w^2}, \tag{3}$$

where $u$ and $V$ are the flow speed and specific volume of the mixture, $V_w$ and $V_g$ are the specific volume of liquid water and vapor at temperature $T$, $u^*$ is the velocity of the water, and $V_{w3}$ its specific volume below $Z^*$, where no flashing has taken place.

The energy equation is

$$\left[\frac{X}{V_w} h_w + \frac{(1-X)}{V_g} h_g\right] u = \frac{h_{w3}}{V_{w3}} u^*, \tag{4}$$

where $h_w$ and $h_g$ are the specific enthalpy of liquid and vapor, respectively ($h_{w3}$ is the liquid enthalpy at $T_3$). The kinetic and potential energy of the flow has been neglected. Because of the large temperature change due to flashing, the transfer from internal energy to kinetic and potential energy has only a small effect on the overall temperature change and may be neglected (Elder, 1966).

The hydrodynamic losses may be treated by using a friction factor formulation for the momentum balance, and we can write

$$\frac{dp}{dz} = \frac{g}{V} + \lambda \frac{u^2}{4 V r_w}, \tag{5}$$

where we have neglected the momentum of the fluid but include the gravitation effect and friction. The friction factor for single-phase flow in circular pipes is tabulated as a function of Reynolds number and pipe surface roughness (for example, Katz and others, 1959). For geothermal bores, the Reynolds number is usually high ($\approx 10^6$) and the friction factor is then only a function of the surface roughness (Elder, 1966). (A tripling of surface roughness from that for gas-well tubing to that for wrought iron for a typical bore size leads to only a one-fourth increase in friction factor.) The neglect of the fluid momentum is consistent with the assumption of low Mach number flows. Although the Mach number can approach 1 in some high-output bores when backpressure is low, the large hydrodynamic resistance due to friction is more than adequate to limit the flow without need to appeal to sonic flow at the exit. Sonic flow at the exit is important for relating critical pressures to mass flows (James, 1962), but not for the quantities to be calculated here.

The method of calculation involves a computer program to numerically integrate the equations (Nathenson, 1974). Physically, the value of wellhead pressure and the physical parameters of the system determine the flow rate and distribution of temperature and pressure in the bore. Mathematically, it is much easier to pick a value for the bottom-hole flowing pressure. The flow rate can then be calculated from equation 1. The flashing depth is then calculated from equation 2. The distribution of pressure and temperature in the well can then be obtained by integrating (numerically) equation 5 up the bore in combination with equations 3 and 4. The integration has been done using Simpson's rule (Mathews and Walker, 1965, p. 332), and step sizes are chosen to give plotting accuracy. The thermodynamic properties of saturated water and steam are obtained from a look-up program using a four-point Lagrange interpolation routine (P. C. Doherty, written commun., 1973), and a stored set of steam tables (Keenan and others, 1969). The wellhead pressure is found when the integration has proceeded from $Z = Z^*$ to $Z = 0$. If the chosen value for bottom-hole flowing pressure is too low, the calculation terminates when the well pressure reaches 1 bar at some point below the surface. In the

process of debugging the program, I attempted to check the calculations for Elder's (1966) figure 25 and was unable to verify his results. In checking his calculations, I found that $\eta$-lines shown in his figure 24 are incorrect, and this is why his figure 25 was not reproducible.

## GEOTHERMAL BORE CHARACTERISTICS

### Data for model reservoir and well

To investigate in a systematic manner how the reservoir parameters influence well performance, the variation of pressure with depth in the natural system must be established to specify the aquifer pressure. Since the density of liquid water is primarily a function of temperature, hydrostatic equilibrium combined with the temperature-depth relation recognized by Bodvarsson (1961) and White (1968, fig. 3) for high-temperature hot-water convection systems can be used to calculate the pressure-depth relation. Owing to natural convective overturn, the deep part of these systems has virtually a constant temperature (called the base temperature by Bodvarsson). In the near-surface part of an upflowing system, the hydrostatic pressure has decreased sufficiently to equal the saturated vapor pressure of the liquid water; vapor will then start to form. Above this point, decreasing hydrostatic pressure will cause increasing quantities of vapor to form with a corresponding decrease in temperature. This dependence of temperature on depth is approximated by the reference boiling-point curve (White, 1968, fig. 30; Hass, 1971) with the temperature at the water table fixed by atmospheric pressure at the altitude of the water table. The actual temperature distribution in a convecting hydrothermal systems differs in detail from the above, but this scheme is adequate for purposes of hydrostatic pressure calculations.

The water table is assumed to lie at some distance $H_{wT}$ below the surface of the ground (negative values of $H_{wT}$ would then correspond to overpressured systems such as the geyser basins of Yellowstone National Park described by White and others, 1968). Temperatures below this level are assumed to follow the reference boiling-point curve from 100°C at the water table to the base temperature of the system $T_3$ at a distance $H_{wT} + H_{BP}$ below ground level. Below this level, the temperature is assumed to be uniformly at $T_3$ and the pressure increases with depth at a slope depending on the density of water at $T_3$. The pressure in the aquifer at datum $H$ may then be written as

$$p_3 = SVP_3 + \frac{g}{V_{w3}}\left[H-(H_{wT}+H_{BP})\right]. \qquad (6)$$

Using equation 2 in equation 6, the driving force for flow in the porous medium is

$$p_3 - p_4 = \frac{g}{V_{w3}}\left[Z^*-(H_{wT}+H_{BP})\right]. \qquad (7)$$

Provided that the casing extends below $Z^*$ (so that no flashing occurs in the porous medium), the driving force given by equation 7 is independent of the well depth.

The independent parameters for the problem formulated in this manner are aquifer temperature $T_3$, permeability $K$, aquifer thickness $L$, well radius $r_w$, friction factor $\lambda$, and depth of water table $H_{wT}$. For geothermal bores, a reasonable radius of 12.7 cm and a surface roughness of 0.008 cm yield a friction factor of $\lambda = 0.015$. The ratio of drainage radius to well radius ($r_e/r_w$) will be taken as 500. The actual value matters little as long as it is large. A reasonable value for uncased length is 300 m, which will be used throughout.

### Characteristics of a good geothermal bore

For a representative well in a good geothermal system, we assume an aquifer temperature of 250°C and a system permeability of 50 mD (millidarcys). Some of the details of pressure and temperature in this system for water table at the surface are shown in figure 2 and at depths of 100 m in figure 3 and 300 m in figure 4. Curves $A$ of these figures are the initial system pressure and temperature. The initial temperature attains the base temperature at and below 463 m below the water table. Curves $B$ show the pressure and temperature distributions obtained in the mathematical limit obtained by integrating equations 3, 4, and 5 with the mass flow equal to zero. The pressure and temperature distribution curves for a flowing bore neglecting friction can be obtained from curves $B$ by shifting them down the amount needed to obtain the pressure drop in the porous medium for the flow under

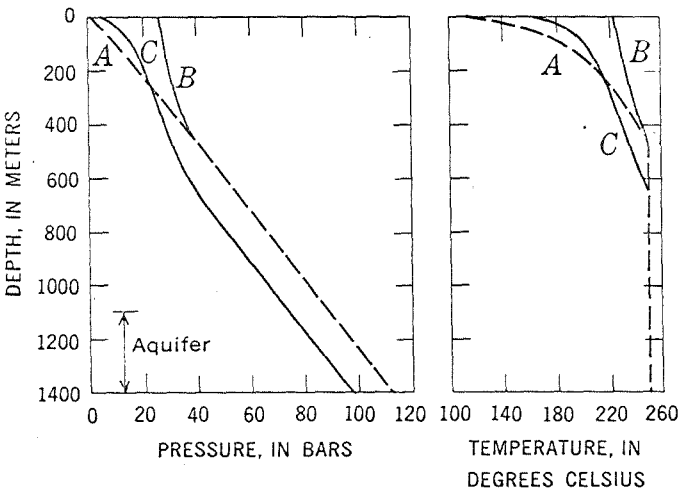


Figure 2.—Pressure and temperature profiles for water table at the surface. Curves $A$, system before discharge; curves $B$, zero-mass-flow limit; curves $C$, mass flow = 168 kg/s, wellhead pressure = 6.2 bars. Reservoir parameters: $T_3 = 250°C$, $K = 50$ mD, $r_e/r_w = 500$. Well parameters: $L = 300$ m, $r_w = 12.7$ cm, $\lambda = 0.015$.

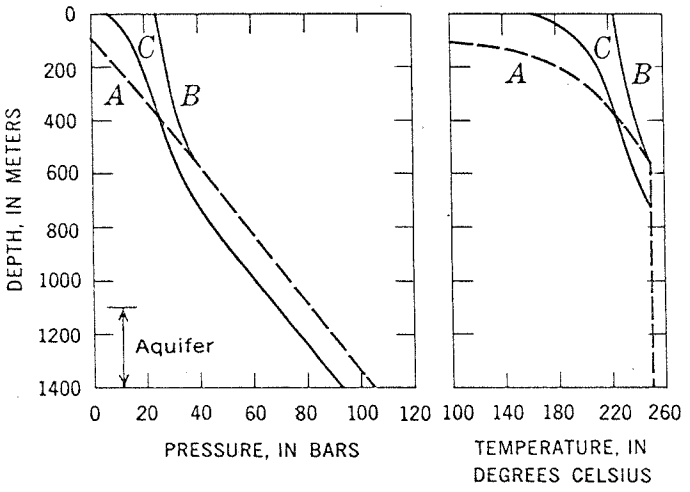


Figure 3.—Pressure and temperature profiles for water table at depth of 100 m. Curves $A$, system before discharge; curves $B$, zero-mass-flow limit; curves $C$, mass flow = 151 kg/s, wellhead pressure = 6.1 bars. Other parameters same as figure 2.

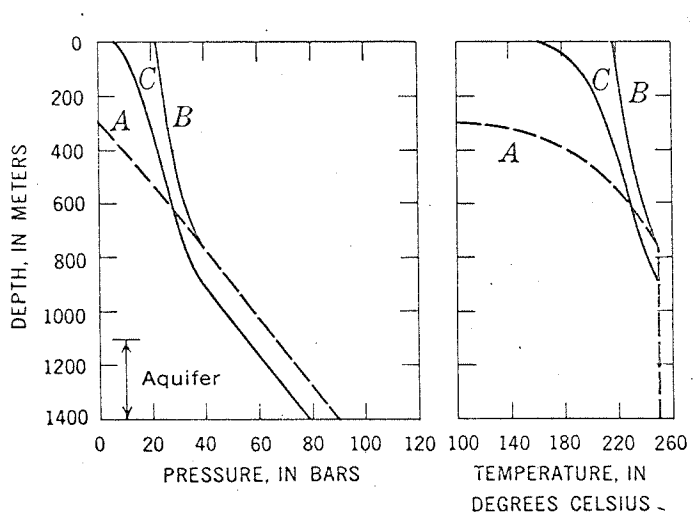


Figure 4.—Pressure and temperature profiles for water table at depth of 300 m. Curves $A$, system before discharge; curves $B$, zero-mass-flow limit; curves $C$, mass flow = 124 kg/s, wellhead pressure = 6.1 bars. Other parameters same as figure 2.

consideration (by using eqs 7 and 1). Although the conditions assumed to calculate curves $B$ cannot occur (dispersed mixture of steam and water with no flow), the curves provide a useful mathematical limit. For flows at high wellhead pressure, the effects of friction should be small and the pressure distribution should be similar to curve $B$ shifted downward. Curve $C$ shows wellhead pressures of approximately production values ($\approx$6 bar). In this example, the hydrodynamic resistance due to the two-phase mixture in the upper part of the bore is large, as shown by the bending over toward the origin of curve $C$ relative to curve $B$ of these profiles, and further reductions in wellhead pressure do not bring corresponding gains in flow rate. Note also the movement of the flash point deeper in the hole with increased flow. A higher water table makes it possible to move the flashing surface deeper relative to its value for zero flow than for the lower water table, and this greater relative movement yields greater flows at the same value of wellhead pressure (compare curves $B$ and $C$ in figure 2 with $B$ and $C$ in 3 and 4).

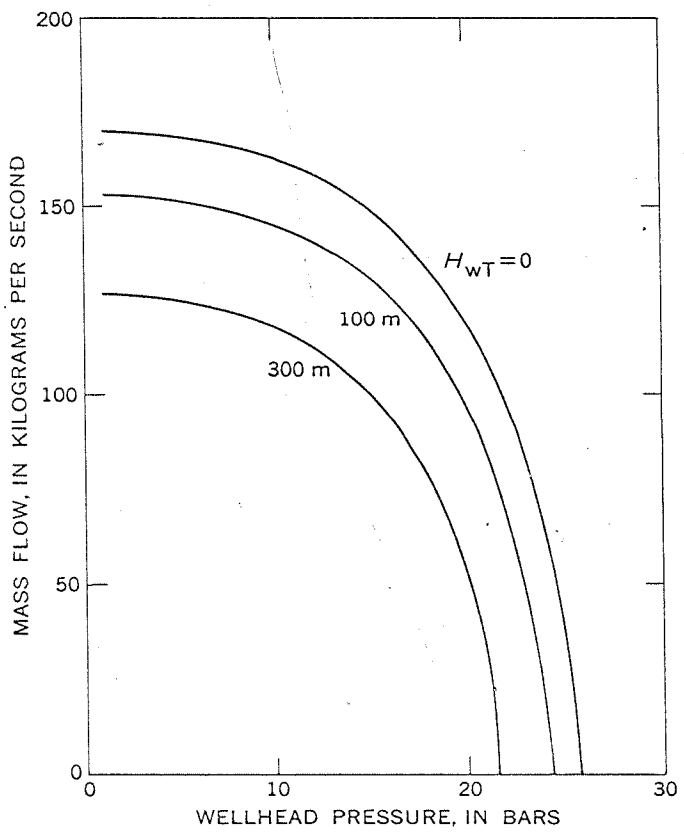


Figure 5.—Mass flow of steam-water mixture as a function of wellhead pressure for three depths to water table ($H_{WT}$). Reservoir and well parameters same as figure 2.

This behavior can be seen more easily in the wellhead curves for mass flow as a function of pressure shown in figure 5 for the three depths to water table, with other conditions held constant. Note that near the no-flow values of wellhead pressure, each decrease in wellhead pressure results in a large increase in mass flow. Near production pressures, however, the large resistance of the flashed mixture due to higher proportion of steam and greater velocity causes the wellhead pressure to have little effect on mass flow. This fact has important implications for finding the value of wellhead pressure that maximizes the flow of useful energy from a geothermal bore.

To calculate the flow of useful energy, we can apply the concept of availability (Jones and Hawkins, 1960, chap. 11;

Bodvarsson and Eggers, 1972). The availability of a system in a given state is defined by Jones and Hawkins as "the maximum amount of useful work which could be obtained from the system-atmosphere combination as the system goes from that state to the dead state while exchanging heat only with the atmosphere." To calculate the available energy as a function of wellhead pressure, we adopt the following scheme. Assume that, at the value of wellhead pressure under consideration, the steam and water of the mixture are separated, the steam is used to produce mechanical work, and the water is discarded. Neglecting the kinetic and potential energy, the specific availability of the steam (availability per unit mass of steam) is

$$y = (h_{g,wh} - T_0 s_{g,wh}) - (h_0 - T_0 s_0) \quad (8)$$

where $T_0$ is the absolute temperature of the cold reservoir, $h_{g,\,wh}$ and $s_{g,\,wh}$ are the enthalpy and entropy of saturated steam at the separation pressure, and $h_0$ and $s_0$ are the enthalpy and entropy of the dead state. The dead state will be taken as saturated liquid at pressures of 0.1 bar (45.8°C) and 1 bar (99.6°C). The ideal power ($E$) available from the bore may then be calculated from

$$E = \eta M y, \quad (9)$$

where $\eta$ is the mass fraction of steam, $M$ is the mass flow of the steam-water mixture, and $y$ is the specific availability of the steam. For a unit mass of total fluid, the steam availability is $\eta y$; this quantity is plotted in figure 6 for water that was liquid at 250°C. The calculation has been carried only to 30 bars because a 250°C bore will not normally be produced at wellhead pressures above this value. The plot shows the result of competition between two factors. Lower wellhead pressures result in higher steam fractions but bring the steam temperature closer to the cold reservoir temperature, thus lowering the availability per unit mass of steam. The competition results in a maximum of availability at a certain separation pressure, as shown. Note also that, with isenthalpic flow, once the aquifer temperature and dead state are fixed, the availability per unit mass of mixture is fixed by the separation pressure. Factors that tend to reduce the flow, such as deeper water table or lower permeability, affect only the quantity of fluids produced, not their specific availability (as long as there is enough flow that heat transfer is negligible).

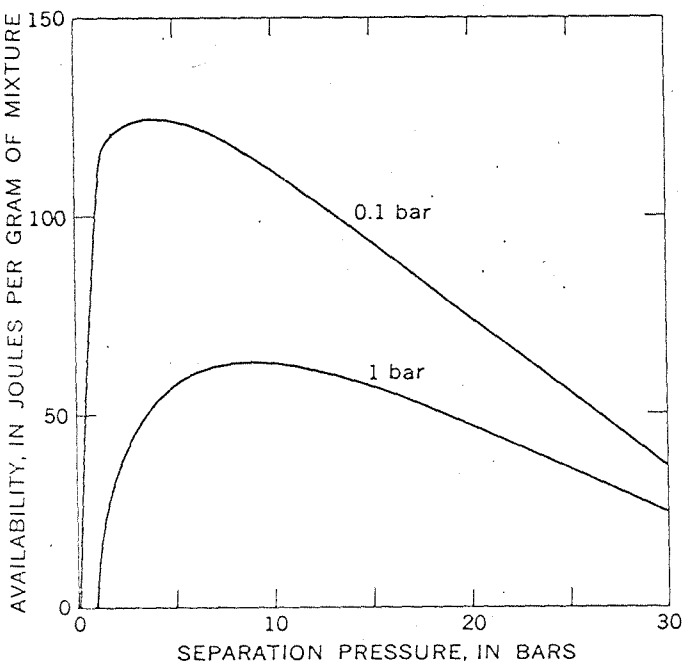


Figure 6.—Availability of steam phase per unit mass of mixture as a function of separation pressure for dead states of saturated liquid at 0.1 bar (45.8°C) and 1 bar (99.6°C) for water initially at 250°C.

Combining this thermodynamic calculation with output characteristic shown in figure 5 for a surface water table ($H_{wT} = 0$), we obtain the ideal power output shown in figure 7. Note that this calculation involves only the Carnot

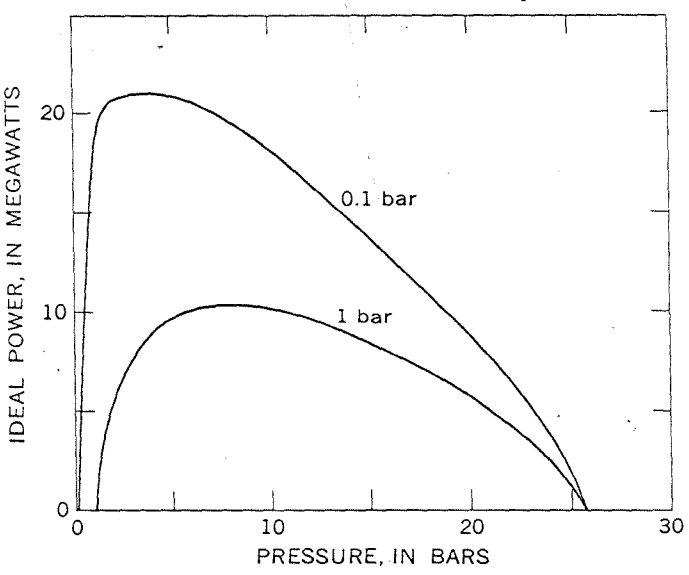


Figure 7.—Ideal output power as a function of separation (= wellhead) pressure for calculated flow shown in figure 5 for water table at surface.

efficiency and does not include any factors for losses in pipeline transmission, turbine losses, and other losses. The curves show the value of optimum wellhead (separation) pressure for maximum energy flow (James, 1967). As this optimum occurs in a flat part of the mass output curve, its location is basically governed by the thermodynamic considerations of figure 6 rather than the calculations of bore mass discharge.

## Parametric investigation of geothermal bore characteristics

To study the effect of the reservoir parameters on well output, a number of wellhead characteristics such as the set

shown in figure 5 can be presented for different values of the parameters. These curves are all fairly similar in shape with the maximum flow and wellhead pressure for zero flow changing their size in response to changes in the reservoir properties. For comparison, a useful quantity is the mass flow for wellhead pressures of 6 bars, corresponding roughly to production conditions at Wairakei. Figure 8 shows the mass flow as a function of reservoir permeability for three depths of water table. For these values of flow the corresponding depth to first flashing is shown. The parameters $L$, $D$, $\lambda$ and $r_e/r_w$ have the same values as in previous calculations. For a system permeability of 100 mD and a surface water table, the flow at a wellhead pressure of 6 bars can then be read from figure 8 as 190 kg/s and the depth of initial flashing as 570 m. The dashed horizontal lines in the lower part of figure 8 show the depths at which the base temperature ($H_{wT}+H_{BP}$) of the system is first reached for each depth to water table. For high permeabilities, the depth to first flashing need only be a little below the reference value in order to obtain the large flows shown. The limiting resistance at these high flow rates is the hydrodynamic resistance in the bores owing to the flow of a two-phase mixture. For low permeabilities, large changes in the depth of first flashing are needed to obtain the flows shown. The lower flow rates force the flash point to move deep enough for the length and weight of the two-phase column to achieve low wellhead pressure before hydrodynamic resistance becomes the controlling mechanism. This can be seen clearly in figure 9, where the pressure distribution is shown for a well in a system where permeability is only 5 mD; curve $C$ shows little bending over at low wellhead pressure as compared with curve $C$ of figure 2. Decreasing the diameter of this well would cause hydrodynamic resistance in the bore to be the limiting factor and would decrease the maximum depth of first flashing, but would also lower the maximum flow rate.

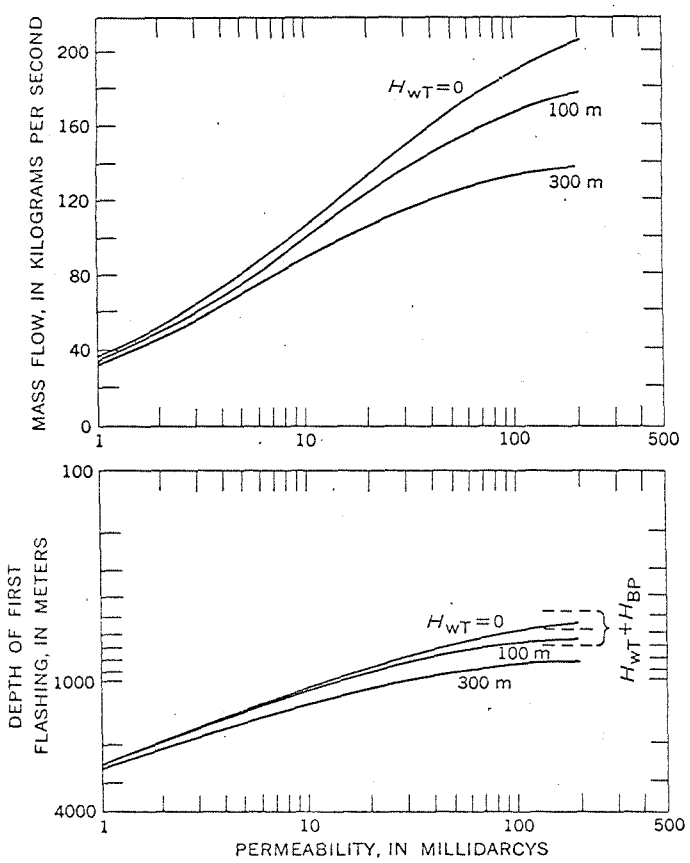


Figure 8.—Mass flow and depth of first flashing for wellhead pressure of 6 bars for range of permeabilities and several depths to water table ($H_{wT}$). Reservoir parameters: $T_3$=250°C, $r_e/r_w$ = 500. Well parameters: $L$=300 m, $r_w$=12.7 cm, $\lambda$=0.015. The dashed horizontal lines show the depth at which the base temperature ($H_{wT}+H_{BP}$) of the system is first reached for each depth to water table.

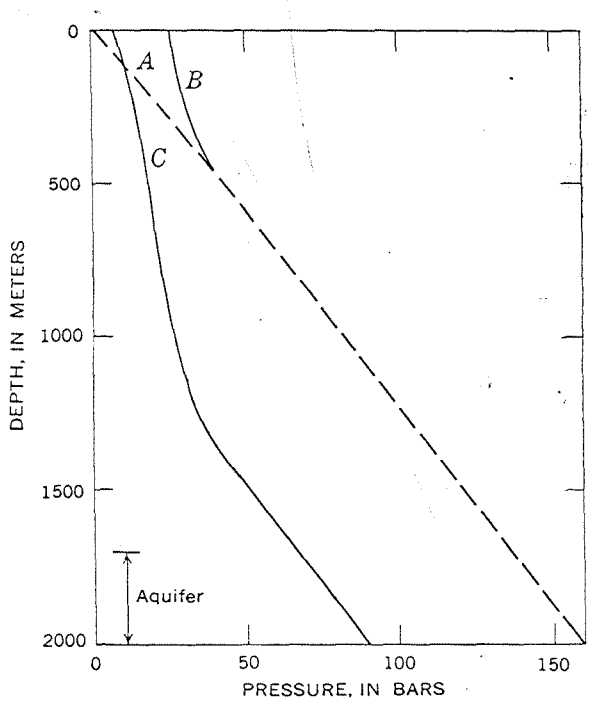


Figure 9.—Pressure profiles for water table at the surface. Low-permeability reservoir. Curve $A$, system before discharge; curve $B$, zero-mass-flow limit; curve $C$, mass flow = 78.3 kg/s, wellhead pressure=7.3 bars. Reservoir parameters: $T_3$ = 200°C, $K$ = 5 mD, $r_e/r_w$=500. Well parameters: $L$=300 m, $r_w$=12.7 cm, $\lambda$=0.015.

To demonstrate the effect of system temperature on well deliverability, flow calculations for a 200°C aquifer are shown in figure 10. The wellhead pressure is still taken as 6 bars. As expected, this lower temperature produces consistently lower flows than were calculated for the 250°C water in figure 8. Note that the depth to water table has a significantly greater effect on the performance, owing to the lower saturated vapor pressure. For the same reason, the flash depths are consistently less than for the hotter water.

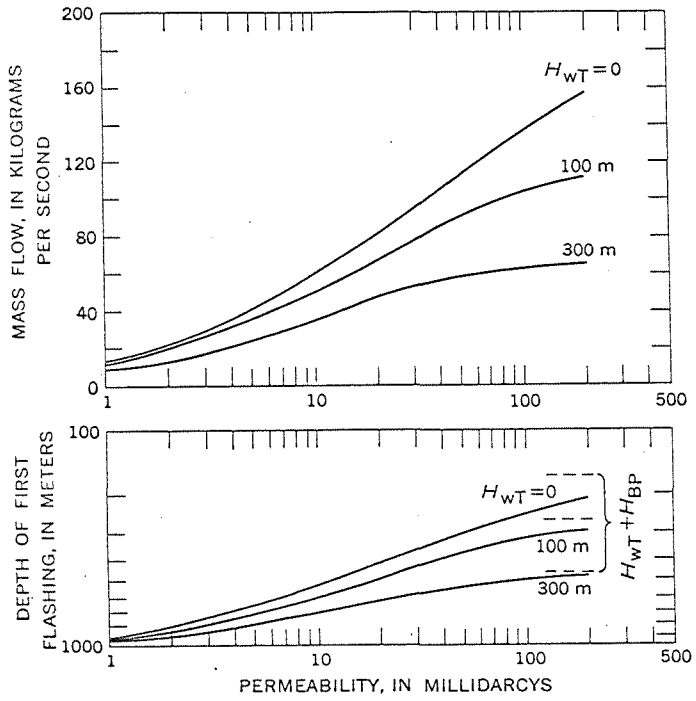


Figure 10.—Mass flow and depth of first flashing for wellhead pressure of 6 bars for range of permeabilities and several depths to water table ($H_{wT}$). Low-temperature aquifer. Reservoir parameters: $T_3$=200°C, $r_e/r_w$=500. Well parameters: $L$=300 m, $r_w$=12.7 cm, $\lambda$=0.015.

## FIELD DATA

Very few data are available on temperature and pressure distributions in flowing geothermal wells, and what is available must be interpreted with care. The first example is some field data obtained by Smith (1958) on the flowing-temperature distribution of Wairakei bore 27. This bore is 610 m deep and is thought to produce from a highly fractured zone about 1 m thick at a depth of 606 m. The bottom-hole shut-in and flowing pressures were measured by Smith, using a 5-cm-diameter tube that was supported at the surface and extended down to 605 m. The tube was supplied with pressurized nitrogen at the surface until the pressure in the tube at the wellhead remained constant. There was essentially no drawdown for this bore, and the gage pressure at 605 m was measured as 54 bars. The physical data used in the calculations are shown in table 1. Because the computer program uses the bottom-hole pressure to set the flow, a large but finite value of permeability was chosen such that drawdown would be very small—less than 1 bar out of the total bottom-hole pressure of 54.5 bars. The two radii shown are for calculations with and without the 5-cm tube in place. Calculating a Reynolds number of around $4\times10^6$ and a relative roughness of $8\times10^{-5}$, we obtain a friction factor of 0.012 (Katz and others, 1959). Using this value for

Table 1.—*Data for bore 27, Wairakei, New Zealand*

| *Parameter* | | *Value* |
|---|---|---|
| Aquifer: | | |
| Temperature $T_3$ | °C | 257 |
| Pressure $P_3$ | bar | 54.5 |
| Permeability $K$ | D | 120 |
| Thickness $L$ | m | 1 |
| Ratio, aquifer radius-well radius, $r_e/r_w$ | | 500 |
| Well: | | |
| Depth $H$ | m | 609.6 |
| Radius $r_w$: | | |
| With tube | cm | 9.8 |
| Without tube | cm | 10.2 |
| Water viscosity $\mu$ | cP | 0.104 |

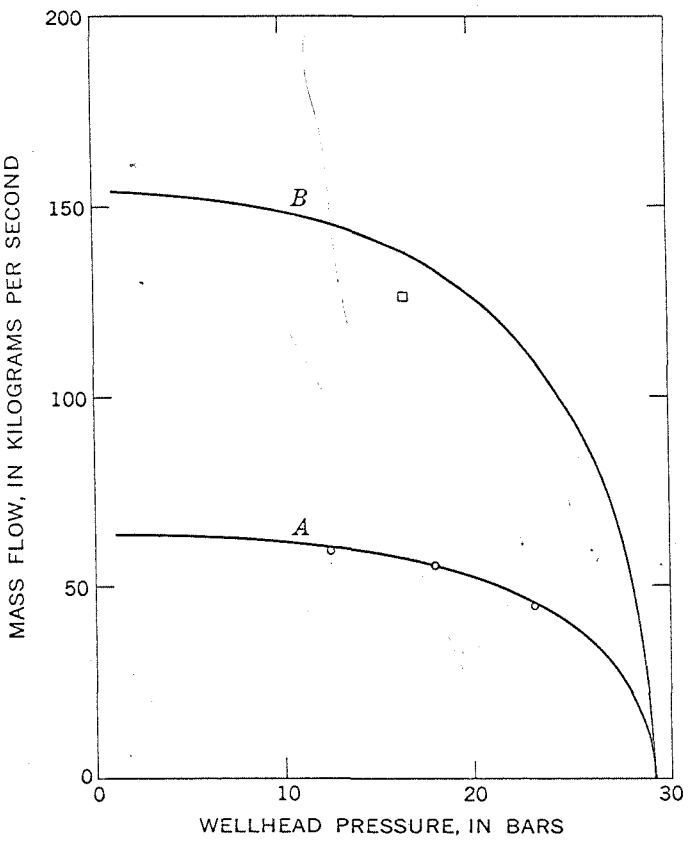


Figure 11.—Mass flows for bore 27, Wairakei, New Zealand. Curve $A$ ($\lambda=0.062$) was calculated with friction factor chosen to match Smith's data (1958), shown as circles; curve $B$ ($\lambda=0.012$) was calculated with friction factor chosen on the basis of estimated surface roughness. Square, data from Grindley (1965) for output in 1959 after bore had been cleaned of mineral deposits. See table 1 for other calculation parameters.

calculation, we obtain flows that are more than double those measured by Smith. Turning around and using the data to obtain a friction factor, a value of 0.062 was required to match the production data measured by Smith, shown in figure 11 as points on curve $A$. Smith obtained corresponding temperatures by lowering a thermocouple into the

5-cm-diameter tubing, and these are shown in figure 12 for the three mass flows and wellhead pressures for which measurements were made. Unfortunately, the validity of the comparison between the measured and calculated temperature data cannot be assessed for the following reasons: (1) The flow sampler used to measure bore outputs was calibrated between September 1957 and November 1958 for large output bores when a larger separator became available, and an output which had been previously been quoted as 75 kg/s became 102 kg/s (R. S. Bolton, written commun., 1973); the quoted outputs in Smith are probably lower than the real outputs, and (2) bore 27 was cleaned of mineral deposits in May 1958 (R. S. Bolton, written commun., 1973).

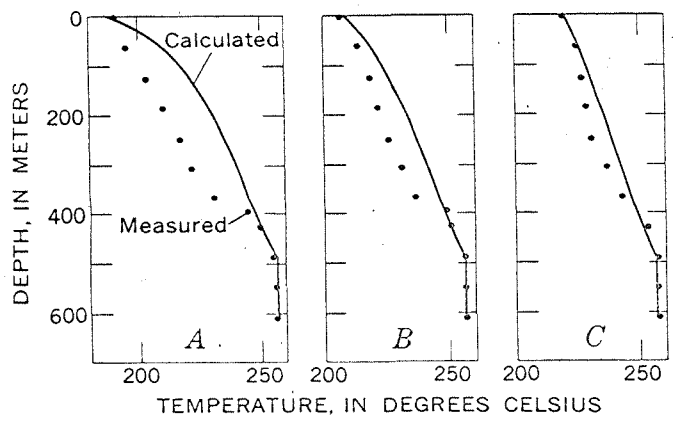


Figure 12.–Measured flowing-temperature profiles in bore 27(dots), Wairakei, New Zealand, compared to calculated values. *A*, Wellhead pressure = 12 bars, mass flow = 59 kg/s (61 kg/s calc). *B*, Wellhead pressure = 18 bars, mass flow = 55 kg/s (55 kg/s calc). *C*, Wellhead pressure = 23 bars, mass flow = 44 kg/s (45 kg/s calc). Parameters as given in table 1 with friction factor = 0.062.

The large effect of mineral deposition can be seen in the flow data for bore 27 reproduced here in table 2 (Grindley, 1965, tables 3 through 16). The cleaning in 1958 is a major cause of the jump in output from 73.4 kg/s in 1957 to 126 kg/s in 1959 with the calibration change causing a change almost as large (the 1957 value is probably closer to 100 kg/s than 75). The quoted flow for 1959 is plotted in figure 11, and the agreement with the predicted wellhead characteristic (curve *B*) is very good. The large difference in outputs from 1957 to 1959 and associated friction factors is due to an area change from mineral deposition and possibly to a change in pipe surface roughness. Photographs in White (1968, figures 39 and 40) of mineral deposits in wells at Steamboat Springs, Nev., show that large quantities can be deposited and that the surface roughness of the deposits can be very large. Going back to the data in table 2, the jump between 1963 and 1964 also is due to a cleaning (R. S. Bolton, written commun., 1973). The inability of bore 27 to regain the 1959 output is probably due to the drop in aquifer pressure that started in 1958–59. By 1961, aquifer pressure at sea-level datum had decreased by approximately 8 bars (Grindley, 1965, figure 29B). The jump in output from 1961 to 1963 is part of a rise that started in November 1961 and peaked about 6 mo later, and for which there is no obvious physical reason (R. S. Bolton, written commun., 1973).

Table 2.–*Mass flows and wellhead pressures for the years 1957, 1959–61, and 1963–65 for bore 27, Wairakei, New Zealand*

[From Grindley, 1965]

| | 1957 | 1959 | 1960 | 1961 | 1963 | 1964 | 1965 |
|---|---|---|---|---|---|---|---|
| Mass flow.....kg/s.. | 73.4 | 126.0 | 69.2 | 45.2 | 70.3 | 84.2 | 73.2 |
| Wellhead pressure ...bar abs.. | 16.2 | 16.2 | 16.9 | 16.2 | 15.2 | 14.9 | 14.8 |

An example of a deep well in a lower temperature aquifer is the U.S. Bureau of Reclamation Mesa 6-1 well in Imperial Valley, Calif. (U.S. Bureau of Reclamation, 1973). The well is 2,443 m deep, has a producing section of 220.4 m (assumed to be equal to aquifer thickness) and an internal casing diameter of 22.05 cm. Steady water flow is given as approximately 250 gal/min (U.S. Bureau of Reclamation, 1973, p. 28). Using the density of water at 198°C, this is approximately 14 kg/s. These data, together with the flowing time of 49 d from figure 7 of the Bureau report and the head recovery data of their figure 17, can be used in Theis' recovery method (DeWiest, 1965, p. 269) to obtain a permeability estimate of 0.94 mD. The permeability can also be calculated form equation 1 with the drawdown obtained from their figure 8. Taking $r_e/r_w = 500$, we obtain 0.85 mD, in good agreement with the other calculation. The friction factor for Reynolds number of around $6\times10^5$ and relative roughness of $7\times10^{-5}$ is 0.014 (Katz and others, 1959). These input data are summarized in table 3.

Calculations based on these data agree well with the measured quantities. The computed flow is 18 percent above the estimated value and the computed depth of first flashing for discharge at atmospheric pressure is within 22 percent of the actual depth. Because the correct friction factors are difficult to predict for these complicated flows, we can use the

Table 3.–*Data for U.S. Bureau of Reclamation Mesa 6-1 well, Imperial Valley, Calif.*

| *Parameter* | | *Value* |
|---|---|---|
| Aquifer: | | |
| Temperature $T_3$ | °C.. | 198 |
| Pressure $p_3$ | bar.. | 220.6 |
| Permeability $K$ | mD.. | 0.85 |
| Thickness $L$ | m.. | 220.4 |
| Ratio, aquifer radius-well radius, $r_e/r_w$ | | 500 |
| Well: | | |
| Depth $H$ | m.. | 2443.3 |
| Radius $r_w$ | cm.. | 11 |
| Friction factor $\lambda$ | | 0.014 |
| | | 0.03 |
| Water viscosity $\mu$ | cP.. | 0.134 |

data to calculate the friction factor. With two iterations, the depth of first flashing and mass flow are matched using a friction factor of 0.03. Note that the friction factor had to be doubled to change the depth of first flashing by 22 percent; this quantity, then, is not very sensitive to a chosen friction factor.

Calculated pressure and temperature distributions obtained by using a friction factor of 0.03 are compared with the measured data shown in figure 13. The predicted pressure decline near the depth of first flashing is too slow, whereas that higher in the hole is too rapid. The temperature curve should be a simple transformation of the pressure, but the saturation curve used in the calculations was for pure water, whereas the well fluid has 3 percent total dissolved solids. Although not a major factor, the dissolved solids would affect virtually every aspect of this analysis, including the flow equations and the fluid properties. Its overall effect is somewhat hard to predict and would be worth looking into as flow data on saline, steam-water mixtures becomes available. Another consideration in assessing the comparison in figure 13 is that the model was not designed to accomodate so low a flow rate. The assumption of a finely divided mixture of equal average velocity should be less accurate here, and the relatively close agreement is reassuring.

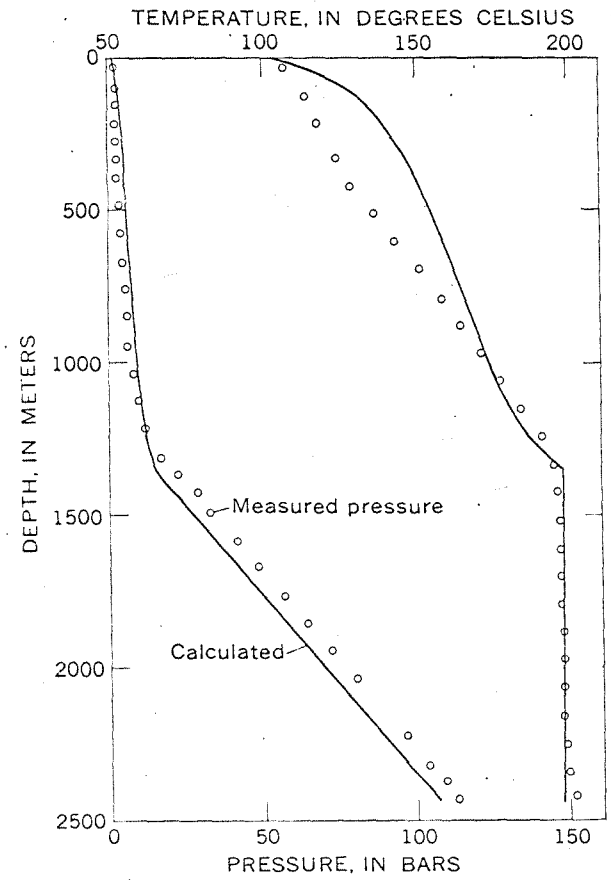


Figure 13.—Flowing-pressure and temperature profiles for U.S. Bureau of Reclamation Mesa 6-1 test well; curves calculated for wellhead pressure of 1 bar absolute and data in table 3 with $\lambda = 0.03$; points measured.

## ACKNOWLEDGMENTS

I would like to thank A. H. Truesdell and D. E. White, U.S. Geological Survey, for their helpful discussions and careful review of the manuscript.

## REFERENCES CITED

Allen, W. F., 1951, Flow of a flashing mixture of water and steam through pipes and valves: Am. Soc. Mech. Engineers Trans., v. 73, p. 257–265.

Bodvarsson, Gunnar, 1951, Report on the Hengill thermal area: Engineers Assoc. Iceland Jour., v. 36, p. 1–48 (in Icelandic; abs. in English).

——1961, Hot springs and the exploitation of natural heat resources in Iceland: Reykjavik, Iceland, State Electricity Authority, Geothermal Department, 20 p.

Bodvarsson, Gunnar, and Eggers, D. E., 1972, The exergy of thermal water: Geothermics, v. 1, p. 93–95.

DeWiest, R. J. M., 1965, Geohydrology: New York, John Wiley, 336 p.

Elder, J. W., 1965, Physical processes in geothermal areas, *in* Lee, W. H. K., ed., Terrestrial heat flow: Am. Geophys. Union, p. 211–239.

Elder, J. W., 1966, Heat and mass transfer in the earth–hydrothermal systems: New Zealand Dept. Sci. and Indus. Research Bull. 169, 115 p.

Grindley, G. W., 1965, The geology, structure, and exploitation of the Wairakei geothermal field, Taupo, New Zealand: New Zealand Geol. Survey Bull. 75, 131 p.

Hass, J. L., Jr., 1971, The effect of salinity on the maximum thermal gradient of a hydrothermal system at hydrostatic pressure: Econ. Geology, v. 66, p. 940–946.

James, Russell, 1962, Steam-water critical flow through pipes: Inst. Mech. Engineers Proc., v. 176, p. 741–748.

——1967, Optimum wellhead pressure for geothermal power: New Zealand Eng., v. 22, p. 221–228

——1968, Pipeline transmission of steam-water mixtures for geothermal power: New Zealand Eng., v. 23, p. 55–61.

Jones, J. B., and Hawkins, G. A., 1960, Engineering thermodynamics: New York, John Wiley, 724 p.

Katz, D. L., Cornell, D., Kobayashi, R., Poettmann, F. H., Vary, J. H., Elenbaas, J. R., and Weinaug, C. F., 1959, Handbook of natural gas engineering: New York, McGraw Hill, 802 p.

Keenan, J. H., Keyes, F. G., Hill, P. G., and Moore, J. G., 1969, Steam tables. Thermodynamic properties of water including vapor, liquid, and solid phases: New York, John Wiley, 162 p.

Muskat, M., 1946, The flow of homogeneous fluids through porous media: Ann Arbor, J. W. Edwards, 763 p.

Mathews, J., and Walker, R. L., 1965, Mathematical methods of physics: New York, W. A. Benjamin, 475 p.

Nathenson, Manuel, 1974, Flashing flow in hot water geothermal wells: computer program: NTIS PB-233 123, 33 p.

Smith, J. H., 1958, Production and utilization of geothermal steam: New Zealand Engineering, v. 13, p. 354–375.

U.S. Bureau of Reclamation, 1973, Test well Mesa 6-1: Geothermal resources investigations, U.S. Dept. Interior Spec. Rept., 44 p.

White, D. E., 1968, Hydrology, activity, and heat flow of the Steamboat Springs thermal system, Washoe County, Nevada: U.S. Geol. Survey Prof. Paper 458-C, 109 p.

White, D. E., Muffler, L. J. P., Truesdell, A. H., and Fournier, R. O., 1968, Preliminary results of research drilling in Yellowstone thermal areas: Am. Geophys. Union Trans., v. 49, p. 358.